European Journal of Radiology 118 (2019) 81–87

Contents lists available at ScienceDirect

European Journal of Radiology

journal homepage: www.elsevier.com/locate/ejrad

Research article

Radiomic analysis of multiparametric magnetic resonance imaging for differentiating skull base chordoma and chondrosarcoma

Longfei Li[a,b,1], Ke Wang[c,d,1], Xiujian Ma[c,d,1], Zhenyu Liu[b,e], Shuo Wang[b], Jiang Du[f], Kaibing Tian[c,d], Xuezhi Zhou[g], Wei wei[g], Kai Sun[g], Yusong Lin[a,h,**], Zhen Wu[c,d,***], Jie Tian[b,e,g,i,*]

[a] Collaborative Innovation Center for Internet Healthcare, Zhengzhou University, Zhengzhou, Henan, 450052, China
[b] CAS Key Laboratory of Molecular Imaging, Institute of Automation, Chinese Academy of Sciences, Beijing, 100190, China
[c] Department of Neurosurgery, Beijing Tian Tan Hospital, Capital Medical University, Beijing, China
[d] China National Clinical Research Center for Neurological Diseases, Beijing, 100050, China
[e] University of Chinese Academy of Sciences, Beijing, 100080, China
[f] Department of Neuropathology, Beijing Neurosurgical Institute, Beijing, Dongcheng Distract, 100050, China
[g] School of Life Science and Technology, Xidian University, Xi'an, Shaanxi, 710071, China
[h] School of Software, Zhengzhou University, Zhengzhou, Henan, 450003, China
[i] Beijing Advanced Innovation Center for Big Data-Based Precision Medicine, School of Medicine, Beihang University, Beijing, China

ARTICLE INFO

Keywords:
Radiomics
Chordoma
Chondrosarcoma
Multiparametric MRI

ABSTRACT

Purpose: Patients with skull base chordoma and chondrosarcoma have different prognoses and are not readily differentiated preoperatively on imaging. Multiparametric magnetic resonance imaging (MRI) is a routine diagnostic tool that can noninvasively characterize the salient characteristics of tumors. In the present study, we developed and validated a preoperative multiparametric MRI-based radiomic signature for differentiating these tumors.

Method: This retrospective study enrolled 210 patients and consecutively divided them into the primary and validation cohorts. A total of 1941 radiomic features were acquired from preoperative T1-weighted imaging, T2-weighted imaging and contrast-enhanced T1-weighted imaging for each patient. The most discriminative features were selected by minimum-redundancy maximum-relevancy and recursive feature elimination algorithms in the primary cohort. The multiparametric and single-sequence MRI signatures were constructed with the selected features using a support vector machine model in the primary cohort. The ability of the novel radiomic signatures to differentiate chordoma from chondrosarcoma were assessed using receiver operating characteristic curve analysis in the validation cohort.

Results: The multiparametric radiomic signature, which consisted of 11 selected features, reached an area under the receiver operating characteristic curve of 0.9745 and 0.8720 in the primary and validation cohorts, respectively. Moreover, compared with each single-sequence MRI signature, the multiparametric radiomic signature exhibited better classification performance with significant improvement ($p < 0.05$, Delong's test) in the primary cohorts.

Conclusion: By combining features from three MRI sequences, the multiparametric radiomics signature can accurately and robustly differentiate skull base chordoma from chondrosarcoma.

1. Introduction

Chordoma and chondrosarcoma are both rare, malignant bone tumors occurring at the skull base, and together account for 1% of intracranial tumors [1,2]. Chordomas are central skull base tumors derived from the remnants of the notochord, with an incidence of approximately 8.4/ten million per year [3]. Chondrosarcomas originate from the synchondroses of the skull base, such as the spheno-occipital

* Corresponding author at: Institute of Automation, Chinese Academy of Sciences, Beijing, 100190, China.
** Corresponding author at: Collaborative Innovation Center for Internet Healthcare, Zhengzhou University, No.75 Daxue Road, Erqi District, Zhengzhou, Henan, 450052, China.
*** Corresponding author at: Department of Neurosurgery, Beijing Tian Tan Hospital, Capital Medical University, Beijing, China.
E-mail addresses: yslin@ha.edu.cn (Y. Lin), wuzhen1966@aliyun.com (Z. Wu), jie.tian@ia.ac.cn (J. Tian).
[1] These authors contributed equally to the work of this manuscript.

https://doi.org/10.1016/j.ejrad.2019.07.006
Received 9 March 2019; Received in revised form 25 June 2019; Accepted 4 July 2019

suture or petroclival suture, are often off-midline, and have an incidence of less than 2/ten million per year [4]. Currently, the standard treatment for both types of tumors is surgical resection combined with or without adjuvant radiotherapy [5]. However, skull base surgery is highly challenging owing to the inaccessibility of the tumors and their close proximity to vital structures such as the brainstem, cranial nerves, and major vessels. Therefore, some studies have suggested that maximal safe surgical resection followed by adjuvant radiotherapy may result in a relatively good prognosis for chondrosarcoma of the skull base [6,7]. For chordoma, owing to its high recurrence rate [8], gross total resection followed by adjuvant radiotherapy is advocated to achieve better long-term survival [9]. Therefore, preoperative discrimination of these two tumors may assist treatment planning and decision-making. Currently, the identification of these two tumors relies mainly on postoperative pathological analysis of the tumor tissue, which includes the use of hematoxylin-eosin staining and evaluation of biomarkers such as gene expression analysis of brachyury, a transcription factor that is highly expressed in chordomas [10,11]. Herein, we describe a preoperative, noninvasive imaging method using radiomics to differentiate these two tumors and thus assist with optimal treatment planning.

Owing to the similar magnetic resonance imaging (MRI) appearance of the two types of tumors, differentiating them using preoperative images remains challenging [12]. Chordomas and chondrosarcomas of the skull base typically demonstrate a hypointense signal on T1-weighted MRI (T1WI), a hyperintense signal on T2-weighted MRI (T2WI), and no distinct visual differences on contrast-enhanced T1-weighted MRI (CET1) [13,14]. Some studies have indicated that diffusion-weighted MRI (DWI) may facilitate assessment of these tumors, and that apparent diffusion coefficient (ADC) values could be used to distinguish skull base chordoma and chondrosarcoma [12,15], though their small sample size, lack of a specified ADC cutoff value, and lack of independent validation make the implementation of this method difficult.

Radiomics is an emerging tool that uses artificial intelligence in the evaluation of medical imaging to achieve improved diagnostic accuracy, and its growing use has received wide attention [16]. It employs an approach that extracts a large number of quantitative features from medical images to thoroughly characterize a region of interest, such as a tumor [17–19]. These extracted features may reflect the characteristics of the underlying pathophysiology, facilitating the evaluation of tumor heterogeneity [20]. A key objective is to generate image-driven signatures as a diagnostic tool that can provide insights into tumor biology and thus better support clinical decision-making [20,21]. In recent years, radiomics has been successfully applied to differentiate different types of tumors involving the eyes, lymph nodes, and lungs [22–24]. However, a reliable predictive radiomics method to differentiate skull base chordoma from chondrosarcoma has not yet been developed.

The aim of our study was to develop and validate a multiparametric MRI radiomic signature that facilitates the differentiation of skull base chordoma and chondrosarcoma. In our study, we used an emerging quantitative analysis approach to differentiate tumors, and then evaluated the robustness of the signature with an independent validation set. Furthermore, we compared the diagnostic performance of the multiparametric signature with each single-sequence MRI signature.

2. Materials and methods

2.1. Patients

This retrospective study was conducted in accordance with the tenets of the Declaration of Helsinki and with ethical approval from our institution's review board. The requirement for informed consent was waived because all patient data were anonymized prior to analysis. A total of 210 consecutive patients (154 skull base chordomas and 56 skull base chondrosarcomas) who underwent MRI between January 2005 and November 2016 were included. These patients were allocated to primary and validation cohorts according to the time of MRI acquisition in a ratio of 2:1; the first 140 patients (103 chordoma and 37 chondrosarcoma) were allocated to the primary cohort, and the last 70 patients (51 chordoma and 19 chondrosarcoma) were allocated to the validation cohort.

The following patients were included: patients (1) with primary skull base chordoma or chondrosarcoma (2) who successfully underwent multiparametric MRI (including T1WI, T2WI and CET1) before surgery and radiotherapy and (3) whose tumor type was confirmed by pathology. Patients with poor image quality due to motion artifacts were excluded.

2.2. Image data acquisition

The images of T1WI, T2WI, and CET1 sequences were acquired using a Magnetom Trio 3 T scanner (Siemens, Erlangen, Germany) with a 12-channel receive-only head coil. The parameters used to acquire these three axial sequences are shown in Supplementary Table 1. The CET1 scan was taken immediately after the rapid intravenous injection of 0.2 mL/kg gadolinium-DTPA (BeiLu Pharmaceutical Co., Ltd, Beijing, China).

2.3. Image segmentation and feature extraction

The radiomics workflow is shown in Fig. 1. A three-dimensional region of interest (ROI) for each skull base tumor was delineated manually by two experienced neurosurgeons (with 5 and 7 years of experience, respectively). The ROIs were segmented slice-by-slice on the axial plane using the three MRI sequences. If the divergence between the segmentations of the two neurosurgeons was less than 5%, the final ROI was defined as the overlap of the two ROIs, and if the divergence was greater than 5%, a third neurosurgeon (with 10 years of experience) made the final decision [25]. All neurosurgeons were blinded to the patient's surgical and pathologic information when delineating these ROIs. Segmentation was performed using ITK-SNAP software (University of Pennsylvania, Philadelphia, PA, USA).

A total of 647 quantitative multiparametric radiomic features were automatically calculated from respective T1WI, T2WI, and CET1 image sequences. These features included four categories: first-order gray-level intensity histograms statistics, tumor size and volume, second-order gray-level texture features, and wavelet features. Detailed information on feature categories is included in Supplementary Table 2. Processing of all features was performed using MATLAB 2015b (MathWorks, Natick, MA, USA).

2.4. Feature selection and radiomic signature building

To ensure that the feature values remained in an appropriate range, we normalized each radiomic feature based on minimum-maximum normalization using the following formula:

$$Normalized\ X_n = \frac{X_n - X_{min}}{X_{max} - X_n}$$

where $X_{\min}$ and $X_{\min}$ represented the respective minimum and maximum values of the feature X_n. Subsequent feature selection and model training were performed based on these normalized features in the primary cohort. Two separate feature selection algorithms were used to select radiomic features to avoid over-fitting of the prediction model. First, radiomic features were selected by the minimum-redundancy maximum-relevancy (MRMR) algorithm, which ranked the features by significance according to mutual information [26]. Next, a recursive feature elimination (RFE) algorithm, was used to select features by recursively considering increasingly smaller sets of features [27].

In the primary cohort, a support vector machine model with a radial

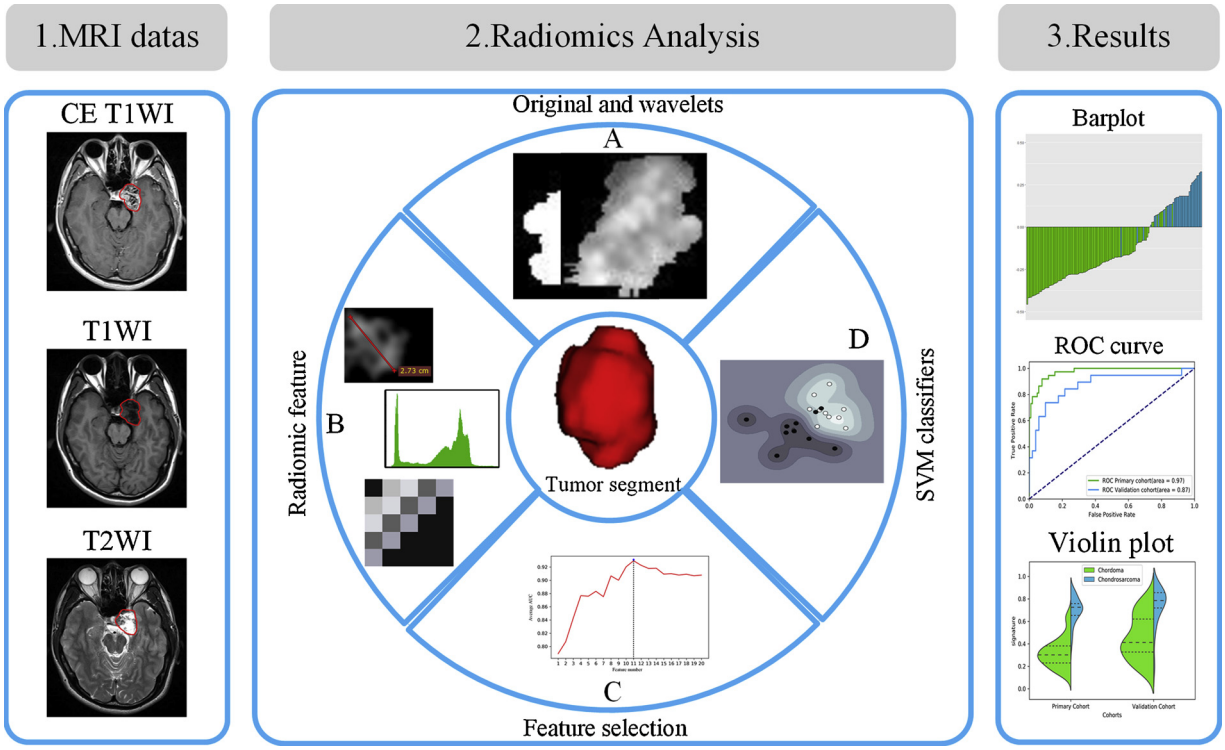

Fig. 1. Radiomics workflow including three steps: A) data collection; B) data analysis, including tumor ROI segmentation, feature extraction, feature selection, and model building; and C) result presentation.

Table 1
Age and sex distribution of chordoma and chondrosarcoma in intra- and inter-class.

Characteristics	Primary cohort (n = 140)			Validation cohort (n = 70)			*P*
	chordoma (n = 103)	chondrosarcoma (n = 37)	*P*	chordoma (n = 51)	chondrosarcoma (n = 19)	*P*	
Age	32.54 ± 13.49	36.51 ± 14.22	0.78	31.32 ± 11.56	36.59 ± 15.56	0.18	0.40
Sex			0.55			0.51	0.07
Male	68	22		25	11		
Female	35	15		26	8		

Note: Chi-Square or Fisher Exact tests, as appropriate, were used to compare the differences in categorical variables, while the independent sample *t*-test was used to compare the differences in age.
(Age, mean ± standard deviation, years).

basis function kernel was trained according to the label and selected features of the two types of tumors. For the model, the parameters of misclassification penalty C and width G were selected from [2^{-5}, 2^{-4}, 2^{-3}, …, 2^{5}] through Grid Search with ten-fold cross-validation loops. The optimal parameters of C and G were determined by maximizing the area under the receiver operating characteristic curve (AUC). The radiomic signature was defined as the probability that the above-mentioned model correctly predicts the type of tumor.

2.5. Validation and comparison of differentiation performance

To assess the differentiation performance of the different radiomic signatures, the prediction AUC, accuracy, sensitivity, and specificity were calculated in the separate primary and validation cohorts. Additionally, the performance of the multiparametric radiomic signature was compared with those of the other three single-sequence radiomic signatures using a Delong test with a Bonferroni correction applied to adjust for multiple comparisons. Based on these results, the predictive signature that yielded the optimal result was selected for subsequent use.

2.6. Statistical analysis

Statistical analyses of all clinical characteristics were conducted with IBM SPSS software (version 19.0, SPSS, US). Continuous variables (e.g., age) were analyzed using Student's *t*-test, and categorical variables (e.g., sex) were analyzed using Pearson's chi-squared test or Fisher's exact test; a two-sided p-value < 0.05 was considered statistically significant.

3. Results

3.1. Patient clinical characteristics

Patient baseline characteristics in the primary and validation cohorts are shown in Table 1. The primary cohort included 90 male patients and 50 female patients, and the mean age and standard deviation were 35.46 ± 14.09 years (range, 2–67 years). The separate validation subgroup included 36 male patients and 34 female patients, and the mean age and standard deviation were 35.23 ± 14.70 years (range, 9–66 years). The clinical characteristics and demographic data of these patients showed no significant differences ($p >$ 0.05) between the

primary and validation cohorts.

3.2. Image segmentation and feature extraction

A total of 1941 three-dimensional radiomic features were obtained from the three MRI sequences. The features of each MRI sequence included 8 shape features, 17 first-order gray-level intensity histogram statistics, 54 s-order gray-level texture features, and 568 wavelet features. These radiomic features used are shown in Supplementary Appendix S1.

3.3. Feature selection and radiomic signature building

After using the MRMR algorithm to eliminate redundant features, the top ten percent of features were input into the RFE algorithm, finally resulting in 11 features used to construct the multiparametric radiomic signature. The details of the selected features are shown in Supplementary Table 3.

The optimal model parameters C and G were to set at 2^{-1} and 2°, respectively, by ten-fold cross-validation in the primary cohort. Each single-sequence MRI radiomic signature was developed in the same manner as that used for construction of the multiparametric radiomic signature.

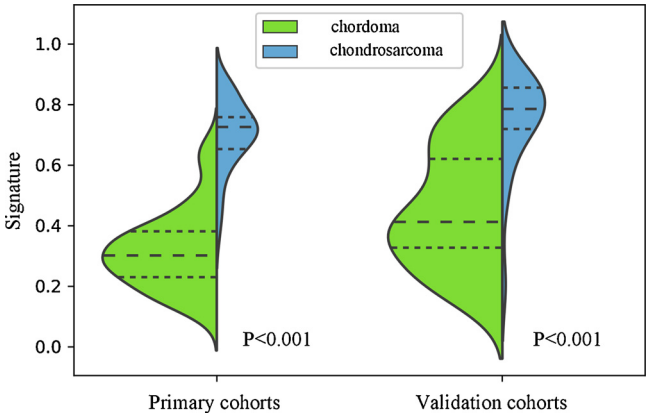

Fig. 3. Violin plot depicting the distribution of the multiparametric radiomic signatures in skull base chordoma and chondrosarcomas. In each cohort, the difference between the signatures of the two tumors were assessed using Student's *t*-test.

3.4. Validation and comparison of the diagnostic performance

The receiver operating characteristic (ROC) curves in Fig. 2(A–D) show the performance of the different radiomic signatures used to differentiate between skull base chordoma and chondrosarcoma in the

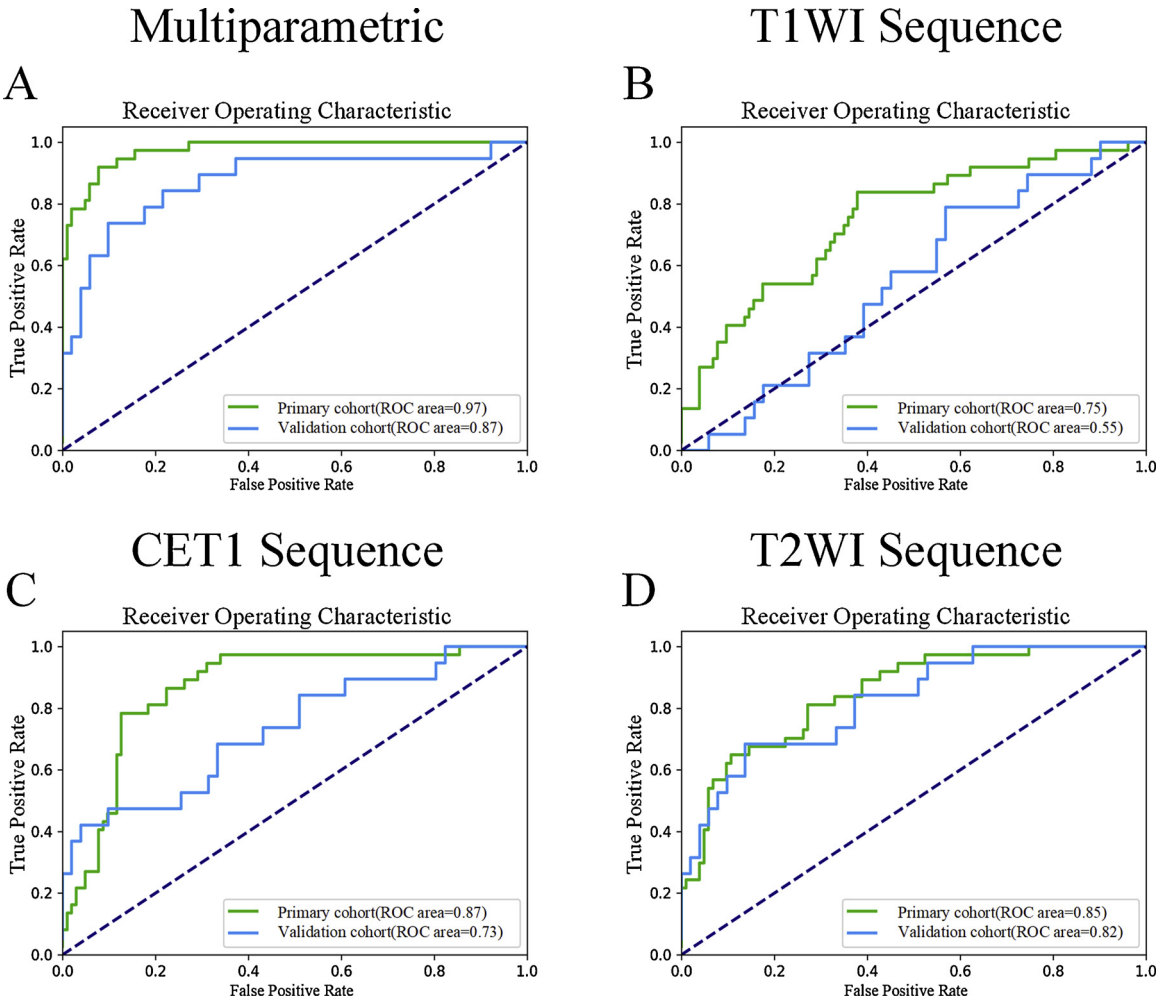

Fig. 2. Receiver operating characteristic (ROC) curves for differentiating skull base chordoma and chondrosarcoma using different radiomic signatures in the primary and validation cohorts. (A) ROC curves of the multiparametric radiomic signature. (B) ROC curves of the radiomic signature derived from T1WI. (C) ROC curves of the radiomic signature derived from CET1. (D) ROC curves of the radiomic signature derived from T2WI.

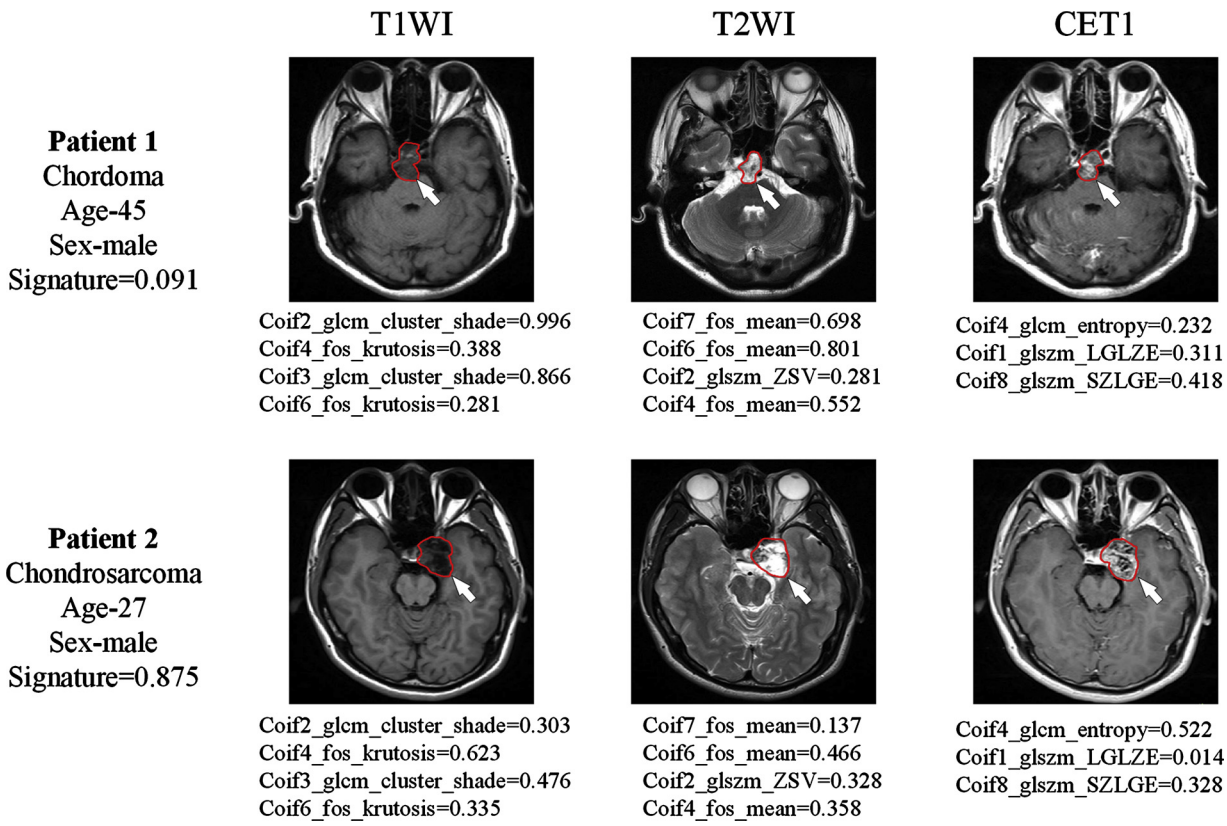

Fig. 4. Illustration of two patients with chondrosarcoma/chordoma showing multiple MRI sequences, clinical characteristics, and multiparametric radiomic signatures.

two cohorts. The multiparametric radiomic signature differentiated the two tumors with an AUC of 0.9745 (95% confidence interval [CI], 0.9668-0.9823) and a classification accuracy of 92.14% (95% CI, 90.48%–93.78%) in the primary cohort. In the validation cohort, the multiparametric radiomic signature yielded an AUC of 0.8720 (95% CI, 0.8440-0.9007) and a classification accuracy of 72.85% (95% CI, 70.24%–75.60%). Barplots depicting the differentiation performance of the multiparametric radiomic signature in the primary and validation cohorts are shown in Supplementary Fig. 1. The multiparametric radiomic signature had a sensitivity of 91.89% (95% CI, 88.66%–95.20%) in the primary cohort and 89.47% (95% CI, 85.74%–93.11%) in the validation cohort, and the specificity was 92.23% (95% CI, 90.26%–94.14%) and 66.67% (95% CI, 63.41%–70.06%) in the primary and validation cohorts, respectively. The distribution of multiparametric signatures of the patients is shown in Fig. 3, which showed a significant difference between chordoma and chondrosarcoma ($p < 0.001$ in both cohorts) (Fig. 4).

The AUC, accuracy, sensitivity, specificity, and detailed performance comparison data for the radiomic signatures are shown in Table 2. The results indicate that the discriminating performance of the multiparametric radiomic signature was better than that of the three single-sequence MRI radiomic signatures. The differences between the ROC curves of the multiparametric and single-sequence signatures were compared using a Delong test, and the resulting *p*-value was used as the quantitative index [28]. There was a significant difference between the multiparametric signature and each of the three single-sequence signatures in the primary cohort ($p < 0.002$). Furthermore, in the validation cohort, a significant difference was seen between the multiparametric and CET1 signatures ($p = 0.016$), and between the multiparametric and T1WI signatures ($p < 0.001$).

4. Discussion

We demonstrated the value of a preoperative multiparametric MRI-based radiomics method to differentiate skull base chordoma from chondrosarcoma. The proposed multiparametric signature showed excellent performance in both the primary and separate validation cohorts compared with signatures based on a single MRI sequence. We believe that such a multiparametric radiomics technique can enable clinicians to discriminate these two skull base tumors in the preoperative setting and thus plan an appropriate surgical strategy.

In this study, the radiomic signatures from each single MRI sequence provided variable discriminative abilities. The overfitting T1WI signature was not a credible predictor although the AUC was 0.75 in the primary cohort, it was only 0.55 in the validation cohort. Even so, there were still four features selected from the T1WI sequence to construct the multiparametric signature, which suggests that T1WI does assist in strengthening the multiparametric signature. Both the T2WI and CET1 signatures were good predictors, with a respective AUC of 0.73 and 0.82 in the validation cohort. We believe that T2WI and CET1 may contain more useful information in differentiating skull base chordoma from chondrosarcoma compared to T1WI. Similarly, previous studies have also demonstrated that T2WI and CET1 were of outstanding value in the prognosis and grading of chordoma [29,30]. We hypothesized that a radiomics method could differentiate these two tumors, which on standard imaging exhibit both a high T2-weighted signal and heterogeneous contrast enhancement on CET1, and our results show that such a radiomics approach was feasible and successful.

Previous studies have stated that the ADC value of DWI could differentiate skull base chordoma and chondrosarcoma [12,15]. However, these studies excluded from analysis areas of tumor-related hemorrhage, necrosis, and cyst formation. Furthermore, owing to the limited number of patients and the lack of a separate validation dataset, the two studies could not provide a unified proposed cutoff for the ADC value.

Table 2
Comparison of diagnosis performance between multi-parametric radiomic signature and single sequence radiomic signatures in primary and validation cohorts.

Comparisons	Cohorts	Multi-parametric	CET1	T1WI	T2WI
AUC	PCS	0.9745 (0.9668,0.9822)	0.8675 (0.8437,0.8913)	0.7484 (0.7155,0.7832)	0.8470 (0.8200,0.8739)
	VCS	0.8720 (0.8434,0.9007)	0.7317 (0.6945,0.7694)	0.5470 (0.5109,0.5829)	0.8235 (0.7953,0.8524)
Sensitivity (%)	PCS	91.89 (88.66,95.20)	86.49 (82.30,90.49)	54.05 (48.15,60.25)	81.08 (76.34,85.88)
	VCS	89.47 (85.74,93.02)	52.63 (46.79,58.57)	0.00 (0.00,0.00)	89.47 (86.05,93.14)
Specificity (%)	PCS	92.23 (90.26,94.14)	73.79 (70.60.77.03)	77.67 (74.75,80.74)	68.93 (65.57,72.29)
	VCS	66.67 (63.41,70.06)	70.59 (67.42,73.84)	98.04 (96.98,99.05)	47.06 (43.25,50.71)
Accuracy (%)	PCS	92.14 (90.48,93.78)	77.14 (74.54,79.75)	71.42 (68.80,74.25)	72.14 (69.28,75.02)
	VCS	72.85 (70.24,75.60)	65.71 (62.82,68.70)	71.42 (68.48,74.21)	58.57 (55.46,61.67)
P	PCS		**0.002**	**0.001**	**0.001**
	VCS		**0.016**	**0.001**	0.300

Abbreviations: PCS Primary Cohort Signature; VCS Validation Cohort Signature; AUC area under receiver-operating characteristic curve; T1WI T1-weighted MRI sequence. T2WI T2-weighted MRI sequence. CET1 = contrast enhancement T1WI sequence.
Note: P-value refers to the significance among the difference of the AUCs between the multi-parametric radiomic signature and the other single sequence signature by Delong test.
(95% confidence interval).

In this study, we performed three-dimensional tumor segmentation in each single MRI sequence throughout the entire tumor without any form of pre-processing so as to exclude areas of hemorrhage, necrosis, or cyst formation. Using radiomics, the ROI assessment encompasses multiple areas of the tumor and thus provides more comprehensive information about the tumor [31–33].

Our final results showed that all of the selected features belong to different Coiflet wavelet filtered images, which are high-dimensional image features that have a wide range of applications in radiomics [34,35]. These radiomic features are difficult to decipher with the human eye and show improved differentiation between tumor types. Further details about Coiflet wavelets are shown in Supplementary Appendix S2. Previous studies have shown that chordoma and chondrosarcoma are difficult to differentiate using conventional imaging features on MRI [14,36]. In our study, we found that the high-dimensional wavelet features exhibited a high value in differentiating these tumors. The 11 selected features included five first-order gray-level intensity histogram statistics and six gray-level texture features. These two classes of features have been used in analysis of both computed tomography and MRI images to differentiate a variety of different tumors [23,37]. The most significant feature was “glcm entropy” of the Coif4 wavelet in the CET1 imaging sequence, which measured the distribution of each pixel intensity inside the tumor. Skull base chondrosarcoma showed a higher value in this feature than did skull base chordoma, indicating more uncertainty or complexity of pixel intensity inside the chondrosarcoma ROI. These results indicate that CET1 after Coif4 wavelet transformation showed more complicated tissue distribution of skull base chondrosarcoma compared to chordoma, and this signal is useful in differentiating these two tumors.

Our results show that the discriminant performance of the prediction models on primary cohort is better than that of the validation cohort. This may be caused by the following reasons: 1) Data in the primary cohort are seen by the model during the model training process, however, data in the validation cohort are unknown to the model. Consequently, performance of the model probably drops in the validation cohort. 2) To simulate the prediction process in practice, we used patients diagnosed at earlier time to train the model and used patients diagnosed at latter time to evaluate the model. However, due to the relatively long study period (from 2005 to 2016), patients in the primary cohort and the validation cohort may have some differences, which may cause the performance differences between the two cohorts. This phenomenon is observed in similar studies [38,39]. In this study, we used feature selection method to solve this problem. In the future study, we will collect a larger cohort and improve the radiomics method to train a more robust model.

Our study also has multiple limitations. First, we used a retrospective MRI dataset. The number of patients with chondrosarcoma was small relative to the overall size of the cohort. Additionally, the entire cohort in our study was from a single hospital. In our experimental results, there are some differences in the discriminant performance of the primary and validation cohorts. Patients with metastatic tumors were not included in the current study, and only primary chordoma and chondrosarcoma of the skull base were differentiated.

5. Conclusions

Our study demonstrates that a novel radiomic signature based on preoperative multiparametric MRI can differentiate skull base chordoma and chondrosarcoma accurately and robustly. This multiparametric radiomic signature could be used as a valuable clinical tool to assist clinicians in differentiating a patient’s tumor type before surgery and thus develop an individualized treatment plan.

Acknowledgements

This paper is supported by the National Natural Science Foundation of China under Grant No. 81772009, 81227901, 81772012, 81672506 and 81802683, the National Key Research and Development Plan of China under Grant Nos. 2017YFA0205200, Scientific and Technological Research Project of Henan Province Grant No.182102310162, the Youth Innovation Promotion Association CAS Grant No. 2019136, the Beijing Natural Science Foundation under Grant No. 7182109, Beijing Municipal Science & Technology Commission Nos. Z171100000117023, Z161100002616022, Chinese Academy of Sciences under Grant No. GJJSTD20170004 and QYZDJ-SSW-JSC005. Special Found for The Talents of Beijing Grant No. 2016000021469G212.

Appendix A. Supplementary data

Supplementary material related to this article can be found, in the online version, at doi:https://doi.org/10.1016/j.ejrad.2019.07.006.

References

[1] J.J. Van Gompel, J.R. Janus, Chordoma and chondrosarcoma, Otolaryngol. Clin. North Am. 48 (2015) 501–514.
[2] Y. Kitamura, H. Sasaki, K. Yoshida, Genetic aberrations and molecular biology of skull base chordoma and chondrosarcoma, Brain Tumor Pathol. 34 (2017) 1–13.
[3] J.J. Gompel, Janus J.R. Van, Chordoma and chondrosarcoma, Otolaryngol. Clin. North Am. 48 (2015) 501–514.
[4] D. Li, J.C. Weng, G.J. Zhang, S.Y. Hao, J. Tang, L.W. Zhang, et al., Proposed treatment paradigm for intracranial chondrosarcomas based on multidisciplinary coordination, World Neurosurg. 109 (2018) e517–e530.
[5] J.S. Whelan, L.E. Davis, Osteosarcoma, chondrosarcoma, and chordoma, J. Clin. Oncol. 36 (2018) JCO2017751743.
[6] M. Awad, A.J. Gogos, A.H. Kaye, Skull base chondrosarcoma, J. Clin. Neurosci. 24 (2016) 1–5.
[7] A.L. Holtzman, R.L. Rotondo, M.S. Rutenberg, D.J. Indelicato, C.E. Mercado, D. Rao, et al., Proton therapy for skull-base chondrosarcoma, a single-institution outcomes study, J. Neurooncol. 142 (2019) 557–563.
[8] E.R. Gatfield, D.J. Noble, G.C. Barnett, N.Y. Early, A.C.F. Hoole, N.F. Kirkby, et al., Tumour volume and dose influence outcome after surgery and high-dose photon radiotherapy for chordoma and chondrosarcoma of the skull base and spine, Clin. Oncol. R. Coll. Radiol. (R Coll Radiol.) 30 (2018) 243–253.
[9] L. Wang, Z. Wu, K. Tian, K. Wang, D. Li, J. Ma, et al., Clinical features and surgical outcomes of patients with skull base chordoma: a retrospective analysis of 238 patients, J. Neurosurg. 127 (2017) 1257–1267.
[10] S. Vujovic, S. Henderson, N. Presneau, E. Odell, T.S. Jacques, R. Tirabosco, et al., Brachyury, a crucial regulator of notochordal development, is a novel biomarker for chordomas, J. Pathol. 209 (2006) 157–165.
[11] H. Kano, A. Niranjan, L.D. Lunsford, Radiosurgery for chordoma and chondrosarcoma, Prog. Neurol. Surg. 34 (2019) 207–214.
[12] T. Welzel, E. Meyerhof, M. Uhl, K. Huang, A.V. Deimling, K. Herfarth, et al., Diagnostic accuracy of DW MR imaging in the differentiation of chordomas and chondrosarcomas of the skull base: a 3.0-T MRI study of 105 cases, Eur. J. Radiol. (2018).
[13] A.K. Bag, P.R. Chapman, Neuroimaging: intrinsic lesions of the central skull base region, Seminars in Ultrasound, CT, and MR, (2013), pp. 412–435.
[14] U. Müller, R.A. Kubik-Huch, C. Ares, E.B. Hug, R. Löw, A. Valavanis, et al., Is There a Role for Conventional MRI and MR Diffusion-weighted Imaging for Distinction of Skull Base Chordoma and Chondrosarcoma? (2016), p. 57.
[15] K.W. Yeom, R.M. Lober, B.C. Mobley, G. Harsh, H. Vogel, R. Allagio, et al., Diffusion-weighted MRI: distinction of skull base chordoma from chondrosarcoma, Am. J. Neuroradiol. 34 (2013) 1056–1061.
[16] Z. Liu, S. Wang, D. Dong, J. Wei, C. Fang, X. Zhou, et al., The applications of radiomics in precision diagnosis and treatment of oncology: opportunities and challenges, Theranostics 9 (2019) 1303–1322.
[17] P. Lambin, E. Rios-Velazquez, R. Leijenaar, S. Carvalho, Stiphout RGPMV, P. Granton, et al., Radiomics: extracting more information from medical images using advanced feature analysis, Eur. J. Cancer 48 (2012) 441–446.
[18] V. Kumar, Y. Gu, S. Basu, A. Berglund, S.A. Eschrich, M.B. Schabath, et al., Radiomics: the process and the challenges, Magn. Reson. Imaging 30 (2012) 1234–1248.
[19] R.J. Gillies, P.E. Kinahan, H. Hricak, Radiomics: images are more than pictures, they are data, Radiology. 278 (2016) 563–577.
[20] Aerts HJWL, E.R. Velazquez, R.T.H. Leijenaar, C. Parmar, P. Grossmann, S. Cavalho, et al., Decoding tumour phenotype by noninvasive imaging using a quantitative radiomics approach, Nat. Commun. 5 (2014) 4006.
[21] R. Sun, E.J. Limkin, M. Vakalopoulou, L. Dercle, S. Champiat, S.R. Han, et al., A radiomics approach to assess tumour-infiltrating CD8 cells and response to anti-PD-1 or anti-PD-L1 immunotherapy: an imaging biomarker, retrospective multicohort study, Lancet Oncol. 19 (2018) 1180–1191.
[22] P. Lambin, R.T.H. Leijenaar, T.M. Deist, J. Peerlings, Jong EECD, J.V. Timmeren, et al., Radiomics: the bridge between medical imaging and personalized medicine, Nat. Rev. Clin. Oncol. 14 (2017) 749.
[23] J. Guo, Z. Liu, C. Shen, Z. Li, F. Yan, J. Tian, et al., MR-based radiomics signature in differentiating ocular adnexal lymphoma from idiopathic orbital inflammation, Eur. Radiol. (2018) 1–10.
[24] C. Shen, Z. Liu, Z. Wang, J. Guo, H. Zhang, Y. Wang, et al., Building CT radiomics based nomogram for preoperative esophageal cancer patients lymph node metastasis prediction, Transl. Oncol. 11 (2018) 815–824.
[25] Y. Li, X. Liu, K. Xu, Z. Qian, K. Wang, X. Fan, et al., MRI features can predict EGFR expression in lower grade gliomas: a voxel-based radiomic analysis, Eur. Radiol. 28 (2017) 1–7.
[26] H. Peng, F. Long, C. Ding, Feature selection based on mutual information: criteria of max-dependency, max-relevance, and min-redundancy, IEEE Trans. Pattern Anal. Mach. Intell. 27 (2005) 1226–1238.
[27] I. Guyon, J. Weston, S. Barnhill, V. Vapnik, Gene selection for cancer classification using support vector machines, Mach. Learn. 46 (2002) 389–422.
[28] E.R. Delong, D.M. Delong, D.L. Clarke-Pearson, Comparing the Areas Under Two or More Correlated Receiver Operating Characteristic Curves: a Nonparametric Approach, (2019).
[29] K. Tian, L. Wang, J. Ma, K. Wang, D. Li, J. Du, et al., MR imaging grading system for skull base chordoma, AJNR Am. J. Neuroradiol. 38 (2017) 1206–1211.
[30] J.P. Ma, K.B. Tian, L. Wang, K. Wang, D. Li, Y. Yang, et al., Proposal and validation of a basic progression scoring system for patients with skull base chordoma, World Neurosurg. 91 (2016) 409–418.
[31] Z. Liu, Y. Wang, X. Liu, Y. Du, Z. Tang, K. Wang, et al., Radiomics analysis allows for precise prediction of epilepsy in patients with low-grade gliomas, Neuroimage Clin. 19 (2018) 271–278.
[32] Z. Tang, Z. Liu, R. Li, X. Yang, X. Cui, S. Wang, et al., Identifying the white matter impairments among ART-naïve HIV patients: a multivariate pattern analysis of DTI data, Eur. Radiol. 27 (2017) 4153–4162.
[33] X. Liu, F. Hou, H. Qin, A. Hao, A CADe system for nodule detection in thoracic CT images based on artificial neural network, Sci. China (Inf. Sci.) 60 (2017) 072106.
[34] Z. Liu, X.Y. Zhang, Y.J. Shi, L. Wang, H.T. Zhu, Z.C. Tang, et al., Radiomics analysis for evaluation of pathological complete response to neoadjuvant chemoradiotherapy in locally advanced rectal Cancer, Clin. Cancer Res. 23 (2017) clincanres.1038.2017.
[35] Y.-q. Huang, C.-h. Liang, L. He, J. Tian, C.-s. Liang, X. Chen, et al., Development and validation of a radiomics nomogram for preoperative prediction of lymph node metastasis in colorectal cancer, J. Clin. Oncol. 34 (2016) 2157–2164.
[36] M.N. Pamir, K. Ozduman, Analysis of radiological features relative to histopathology in 42 skull-base chordomas and chondrosarcomas, Eur. J. Radiol. 58 (2006) 461–470.
[37] L. Frighetto-Pereira, R.M. Rangayyan, G.A. Metzner, P.M. de Azevedo-Marques, M.H. Nogueira-Barbosa, Shape, texture and statistical features for classification of benign and malignant vertebral compression fractures in magnetic resonance images, Comput. Biol. Med. 73 (2016) 147.
[38] J. Wei, G. Yang, X. Hao, D. Gu, Y. Tan, X. Wang, et al., A multi-sequence and habitat-based MRI radiomics signature for preoperative prediction of MGMT promoter methylation in astrocytomas with prognostic implication, Eur. Radiol. 29 (2019) 877–888.
[39] J. Qu, C. Shen, J. Qin, Z. Wang, Z. Liu, J. Guo, et al., The MR radiomic signature can predict preoperative lymph node metastasis in patients with esophageal cancer, Eur. Radiol. 29 (2019) 906–914.